ARTICLE TYPE

Network dimensionalities and thermal expansion properties of metal nitroprussides

Tomoyuki Matsuda,[a] Jungeun Kim[b] and Yutaka Moritomo*[a]

We investigated the thermal expansion properties of metal nitroprussides, $M_A[Fe(CN)_5NO]\cdot zH_2O$ (M_A = Mn, Fe, Co, Ni, Cu, Zn, and Cd), which have various network structures, *i.e.* three-dimensional (3D) cubic ($Fm\bar{3}m$ for M_A = Fe, Co, and Ni), distorted three-dimensional (distorted-3D) orthorhombic (*Pnma* for M_A = Mn, Zn, and Cd), and two-dimensional (2D) orthorhombic (*Amm*2 for M_A = Cu) structures. In
10 the cubic system, in which the unbridged NO groups are randomly distributed, isotropic positive thermal expansion was observed. On the contrary, in the orthorhombic system, in which the unbridged NO groups are uniaxially distributed, positive (negative) thermal expansion was observed along (perpendicular to) the uniaxial direction. We interpreted the characteristic thermal responses in terms of the rotational vibrations of the [Fe(CN)_5NO] units as well as their steric hindrances due to the network dimensionality.

Introduction

15 Thermal expansion properties in network structures are attracting a considerable interest of the materials scientists, due to the possibility of zero/negative thermal expansion properties.[1] Recently, coordination polymer frameworks are found to show
20 negative thermal expansion (NTE) behaviors.[2-6] The NTE behaviors in such framework systems are generally attributed to the flexibility of the structure, in which thermal population of low-energy transverse and/or rotational vibrations of the molecular units. Such a flexibility of the lattice causes interesting
25 physical properties, such as pressure-induced structural phase transition,[7] pressure-induced amorphization,[8] and large Grüneisen parameter.[9] In addition, materials with NTE behaviors are useful in variety of electronics application and as components of high-precision thermometers.

30 Prussian blue type cyanides, $A_xM_A[M_B(CN)_6]_y\cdot zH_2O$ (A = alkali metal ion, M_A = Mn, Fe, Co, Ni, Cu, Zn and Cd, and M_B = Fe, Co, Pt) shows characteristic thermal expansion properties.[4-6] The compounds belong to face-centered cubic ($Fm\bar{3}m$; Z = 4) structures, in which M_A and M_B are bridged by the cyano groups
35 and form a three-dimensional (3D) network structure.[10] The alkali metal cations and water molecules are accommodated in the interstitial sites of the lattice. The thermal expansion coefficient ($b \equiv \mathrm{d}\ln a/\mathrm{d}T$) of the lattice constant a systematically decreases with an increase in a: b = +1.49´10^{-5} K^{-1} for
40 Rb$_{0.49}$Co[Fe(CN)$_6$]$_{0.80}\cdot$3.8H$_2$O (a = 9.943 Å) and b = −0.88´10^{-5} K^{-1} for Cs$_{1.00}$Cd[Fe(CN)$_6$]$_{1.00}\cdot$0.5H$_2$O (a = 10.755 Å). The systematic change in b is well explained by the thermally-induced rotational vibrations of the [Fe(CN)$_6$] units as well as their steric hindrances. According to this scenario, we may significantly
45 control the thermal expansion properties by the modification of the dimensionality of the cyano-bridged network.

In this work, we systematically studied the thermal expansion properties of metal nitroprussides, $M_A[Fe(CN)_5NO]\cdot zH_2O$ (M_A = Mn, Fe, Co, Ni, Cu, Zn, and Cd), in which one of the CN groups
50 are replaced by the NO group. The unbridged NO group modiied the dimensionality of the cyano-bridged network structure. Based on the structural analysis, we classified the network structure into three categories, *i.e.*, 3D cubic ($Fm\bar{3}m$ for M_A = Fe, Co, and Ni), distorted three-dimensional (distorted-3D) orthorhombic (*Pnma*
55 for M_A = Mn, Zn, and Cd), and two-dimensional (2D) orthorhombic (*Amm*2 for M_A = Cu) structures. We found that the variation of the network dimensionality crucially influence the thermal expansion properties. We interpreted the dimensionality-dependence of the thermal expansion in terms of the rotational
60 vibrations of the [Fe(CN)$_5$NO] units as well as their steric hindrances.

Experimental

Powders of $M_A[Fe(CN)_5NO]\cdot zH_2O$ (M_A = Fe, Co, Ni, Cu, Zn, and Cd) were prepared by reacting an aqueous solutions of
65 MnCl$_2\cdot$4H$_2$O, FeCl$_2\cdot$4H$_2$O, CoCl$_2\cdot$6H$_2$O, NiCl$_2\cdot$6H$_2$O, CuCl$_2\cdot$2H$_2$O, ZnCl$_2$, CdCl$_2\cdot$2.5H$_2$O, and Na$_2$[Fe(CN)$_5$NO]$\cdot$2H$_2$O. The precipitated powders were filtered and washed with water and then dried in air. Chemical compositions of the prepared samples were determined by inductively coupled plasma atomic
70 emission spectrometry (ICP-AES) for metal elements and standard microanalytical methods for C, H, and N elements. Elemental analyses showed that the formulas of the obtained compounds were Mn[Fe(CN)$_5$NO]$\cdot$2.1H$_2$O (**Mn**), Fe[Fe(CN)$_5$NO]$\cdot$5.0H$_2$O (**Fe**), Co[Fe(CN)$_5$NO]$\cdot$5.4H$_2$O (**Co**),
75 Ni[Fe(CN)$_5$NO]$\cdot$5.8H$_2$O (**Ni**), Cu[Fe(CN)$_5$NO]$\cdot$2.2H$_2$O (**Cu**), Zn[Fe(CN)$_5$NO]$\cdot$2.0H$_2$O (**Zn**), Cd[Fe(CN)$_5$NO]$\cdot$2.3H$_2$O(**Cd**), respectively: calculated wt% for **Mn**: Mn, 17.80; Fe, 18.09; C, 19.45; N, 27.22; H, 1.37%: found; Mn, 17.55; Fe, 18.10; C,

19.48; N, 27.18; H, 1.31%, calculated wt% for **Fe**: Fe, 30.86; C, 16.60; N, 23.23; H, 2.79%: found; Fe, 30.43; C, 16.71; N, 23.17; H, 2.53%, calculated wt% for **Co**: Co, 15.84; Fe, 15.01; C, 16.14; N, 22.58; H, 2.92%: found; Co, 15.72; Fe, 15.02; C, 16.34; N, 22.34; H, 2.68%, calculated wt% for **Ni**: Ni, 15.17; Fe, 14.86; C, 15.98; N, 22.37; H, 3.02%: found; Ni, 15.24; Fe, 14.85; C, 16.02; N, 22.23; H, 2.86%, calculated wt% for **Cu**: Cu, 19.91; Fe, 17.50; C, 18.82; N, 26.34; H, 1.39%: found; Cu, 19.77; Fe, 17.78; C, 18.97; N, 26.32; H, 1.21%, calculated wt% for **Zn**: Zn, 20.60; Fe, 17.60; C, 18.92; N, 26.48; H, 1.27%: found; Zn, 20.08; Fe, 17.46; C, 19.01; N, 26.46; H, 0.90%, calculated wt% for **Cd**: Cd, 30.40; Fe, 15.10; C, 16.24; N, 22.73; H, 1.25%: found; Cd, 30.22; Fe, 15.27; C, 16.54; N, 22.62; H, 0.81%.

In order to precisely determine a and the space groups of the above-synthesized metal nitroprsusides, X-ray powder-diffraction patterns were measured at the synchrotron-radiation facility, SPring-8. First, powder samples were filled into 0.3 mm$f$ glass capillary. The capillary was put on a Debye-Scherrer camera at the BL02B2 beamline of SPring-8.[11] The wavelength of the X-ray ($\lambda \sim 0.5$Å) was calibrated by the lattice constant of standard CeO_2 powder. The sample temperature was controlled by the cooled nitrogen gas. The exposure time was 5 min. The lattice constants of each compound were refined by the RIETAN-FP proprsam,[12] and the 2θ range used in the Rietveld analyses were $3° – 30°$

Results and discussion

Materials

The metal nitroprussids are known to show several types of crystal structures.[13-30] We performed Rietveld analysis of the synchrotron-radiation X-ray powder diffraction patterns of the obtained compounds, and found that the compounds are classified into three types of crystal structures according to the metal ion (Table 1). We show in Fig. 1 the prototypical diffraction patterns at 300 K together with the results of Rietveld refinements. In the inset of Fig. 1, we depicted schematic crystal structures.

The cubic compounds (**Fe**, **Co**, and **Ni**) show 3D network structures similar to the case of the Prussian blue analogues. Here, we note that the five cyano groups of [Fe(CN)$_5$NO] are bridged to the neighboring M_A while the NO group is unbridged.[27]

On the contrary, the orthorhombic compounds (**Mn**, **Cu**, **Zn**, and **Cd**) have rather complicated network structures (Fig. 2). The **Mn**, **Zn**, and **Cd** compounds show distorted-3D network structure. Within the ab plane (Fig. 2a, left), M_A atoms are surrounded by four cyanide nitrogen atoms of [Fe(CN)$_5$NO], forming cyano-bridged 2D layers (M_A—N—C—Fe). Along the c axis (Fig. 2a, right), one side of M_A is coordinated to cyanide nitrogen atom of [Fe(CN)$_5$NO], while the other side is coordinated to the oxygen atom of the water ligand. That is, the five cyano groups of [Fe(CN)$_5$NO] are bridged to the neighboring M_A, while the NO group is unbridged. Due to the steric confinements between the free NO group of [Fe(CN)$_5$NO], and water ligand of M_A, the cyano-bridged M_A-Fe layers along the ab plane are significantly distorted. The **Cu** compound shows 2D network structure. Within the ab plane (Fig. 2a, left), Cu atoms are surrounded by four cyanide nitrogen atoms of [Fe(CN)$_5$NO]. Along the c axis (Fig. 2a, right), however, both sides of Cu atoms are coordinated to the oxygen atoms of water ligands. That is, the

four CN groups of [Fe(CN)$_5$NO] are bridged to the neighboring Cu in the ab plane while the remaining CN group and the NO group are unbridged along the c axis. The cyano-bridged Cu-Fe layers stack alternately along the c axis, causing 2D network structure.

Table 1 Chemical composition, space group, lattice constant at 100 K for M_A[Fe(CN)$_5$NO]·zH$_2$O.

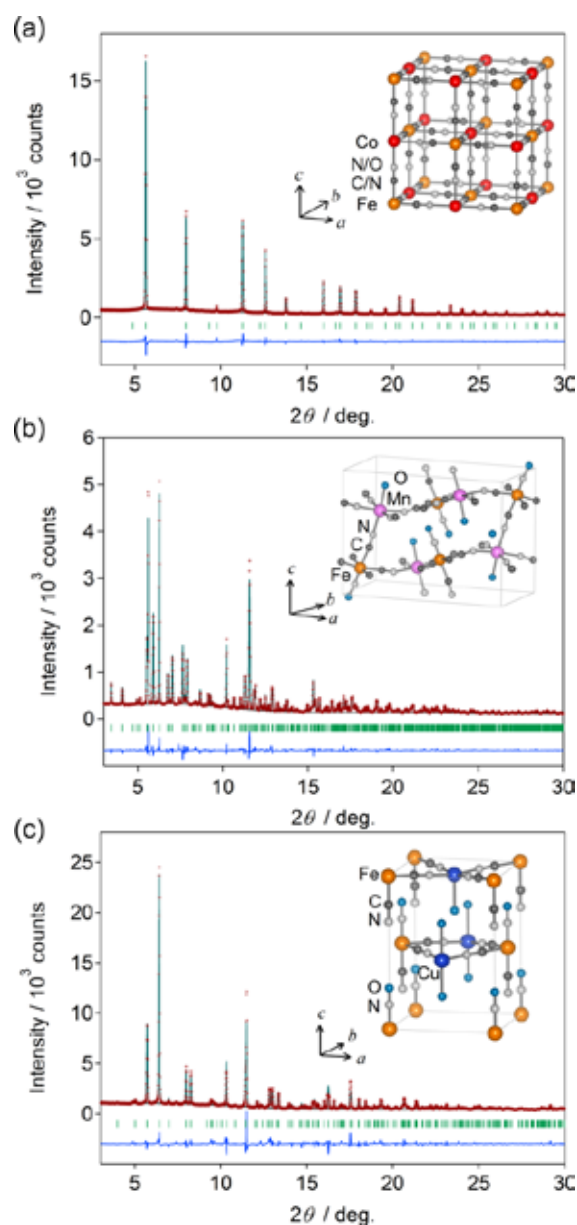|	Space group	Lattice constant / Å		
		a	B	c
Mn[Fe(CN)$_5$NO]·2.1H$_2$O	$Pnma$	14.0371(5)	7.5464(2)	10.4127(3)
Fe[Fe(CN)$_5$NO]·5.0H$_2$O	$Fm3m$	10.3144(3)	–	–
Co[Fe(CN)$_5$NO]·5.4H$_2$O	$Fm3m$	10.2501(2)	–	–
Ni[Fe(CN)$_5$NO]·5.8H$_2$O	$Fm3m$	10.1537(2)	–	–
Cu[Fe(CN)$_5$NO]·2.2H$_2$O	$Amm2$	7.2231(4)	6.9700(4)	10.0850(6)
Zn[Fe(CN)$_5$NO]·2.0H$_2$O	$Pnma$	13.8463(3)	7.4099(2)	10.3789(2)
Cd[Fe(CN)$_5$NO]·2.3H$_2$O	$Pnma$	14.2012(5)	7.6830(3)	10.5029(4)

Fig. 1 X-ray powder diffraction patterns at 100 K and Rietveld analysis of **Co** (a), **Mn** (b), and **Cu** (c). Red dots, black line, and blue line are the observed plots, calculated pattern, and their difference, respectively. Green bars represent the calculated positions of the Bragg reflections. (inset) Schematic illustration of the unit cell.
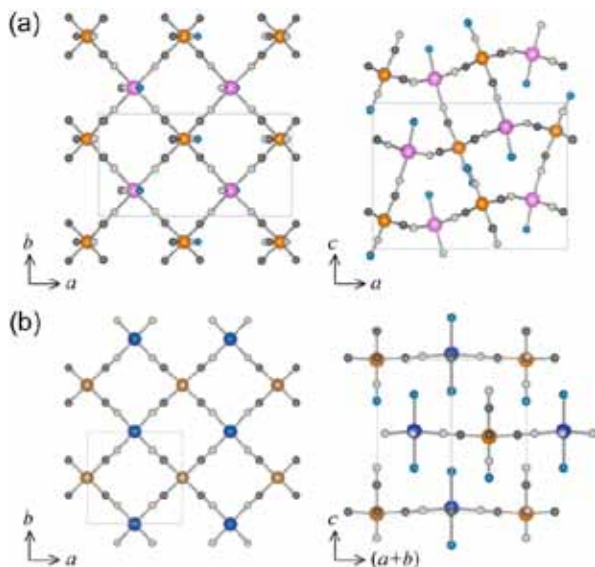

Fig. 2 Schematic crystal structures of distorted-3D network for **Mn**, **Zn**, and **Cd** (a), and 2D network for **Cu** (b). (left) The projection in the *ab* plane. (right) Network structure perpendicular to the *ab* plane.

Thermal expansion properties

We show typical examples of the magnified X-ray diffraction patterns around 422 reflection in **Fe**, **Co**, and **Ni** in Fig. S1 (ESI). The 422 reflection shifts to the high-angle side with decrease in temperature, reflecting PTE. The lattice constants were refined against temperature. The reliable factor R_B ranges from 2.64 to 6.28%. The temperature dependences of the normalized lattice constants are plotted in Fig. 3. We determined *b* by the least-squares fittings; $b = 8.5 \times 10^{-6}$ / K (**Fe**), 6.9×10^{-6} / K (**Co**), and 7.0×10^{-6} / K (**Ni**).
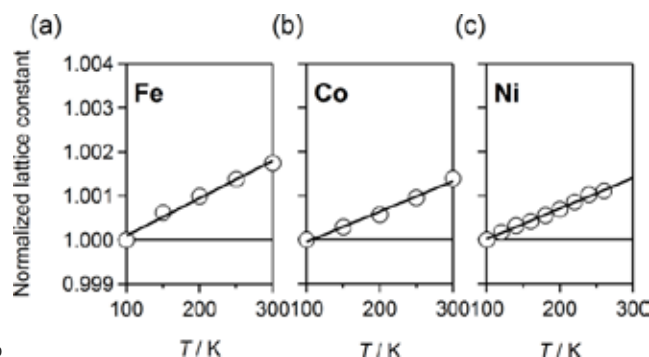

Fig. 3 Temperature dependences of the normalized lattice constants for **Fe** (a), **Co** (b), and **Ni** (c). The lines are the results of the least-squares fittings.

Next, we show in Fig. S2 (ESI) typical examples of the magnified X-ray diffraction patterns around 020, 311, and 212 reflections in **Mn**, **Zn**, and **Cd**, which have distorted-3D networks. The 311 and 212 reflection shift to the high-angle side with decrease in temperature, reflecting positive thermal expansion (PTE). On the contrary, 020 reflection shifts to the low-angle side with decrease in temperature, reflecting NTE along *b* axis. The lattice constants are refined against temperature. The reliable factor R_B ranges from 1.01 to 2.80%. To evaluate the thermal expansion of cyano-bridged *ab* plane, we use the geometrical average of the lattice constants ($a' \equiv a^{1/2} \cdot b^{1/2}$). We show the temperature dependences of a' and *c* values in Fig. 4. We determined *b* by the least-squares fittings. The *b* values are -9.8×10^{-7} / K (*a'*), and 5.35×10^{-5} / K (*c*) for **Mn**, -4.3×10^{-6} / K (*a'*), and 5.19×10^{-5} / K (*c*) for **Zn**, and -3.4×10^{-6} / K (*a'*), and 6.63×10^{-5} / K (*c*) for **Cd**.
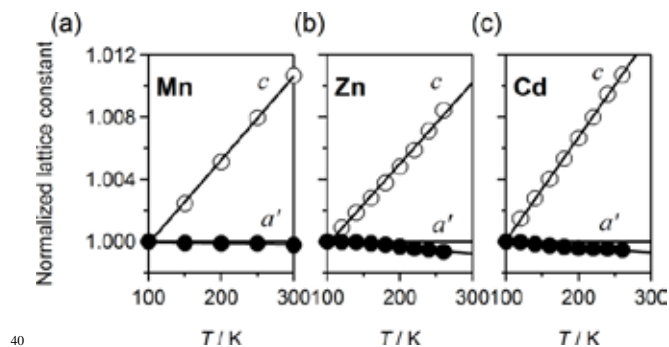

Fig. 4 Temperature dependences of the normalized a' ($\equiv a^{1/2} \cdot b^{1/2}$) and *c* for **Mn** (a), **Zn** (b), and **Cd** (c). The lines are the results of the least-squares fittings.

We show in Fig. S3 (ESI) typical example of magnified X-ray diffraction patterns around 200, 020, 004, and 220 reflections in **Cu**, which have 2D network structure. The 020 and 004 reflection shift to the high-angle side with decrease in temperature, reflecting PTE along *b* and *c* axes. On the contrary, 200 and 220 reflections shift to the low-angle side with decrease in temperature, reflecting NTE along *a* axis and *ab* plane. The lattice constants of **Cu** are refined against temperature, and the reliable factor R_B ranges from 3.08 to 3.41%. To evaluate the thermal expansion of cyano-bridged *ab* plane, we use the geometrical average of the lattice constants ($a' \equiv a^{1/2} \cdot b^{1/2}$). We show in Fig. 5 the normalized values of a' and *c* against temperature. We determined *b* by the least-squares fitting, and the *b* values are -5.2×10^{-6} / K (*a'*), and 1.20×10^{-4} / K (*c*)
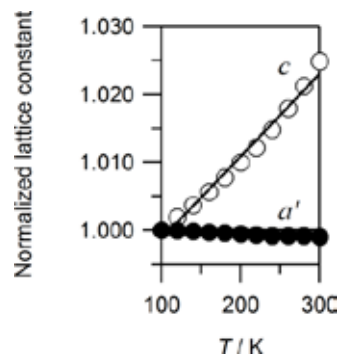

Fig. 5 Temperature dependence of the normalized a' ($\equiv a^{1/2} \cdot b^{1/2}$) and *c* for **Cu**. The lines are the results of the least-squares fittings.

Relation between network dimensionalities and thermal expansion behaviors

Here, we discuss the relation between thermal expansion behavior and dimensionality. We plot the in-plane and out-of-plane components of the thermal expansion against M_A for

$M_A[Fe(CN)_5NO]\cdot zH_2O$. The **Fe**, **Co**, and **Ni** compounds show 3D network, the **Mn**, **Zn**, and **Cd** compounds show distroted-3D network, and the **Cu** compounds shows 2D network.

In the in-plane components (Fig. 6a), the distorte-3D and 2D systems show NTE, while the 3D system shows PTE. This dimensionality dependences of the thermal expansion is well understood by the steric hindrance effect. The origin of the NTE can be ascribed to the rotational vibrations of the $[Fe(CN)_5NO]$ units, analogous to the case of the Prussian blue analgoues.[9] In the distroted-3D and 2D systems, there exist enough spaces for the $[Fe(CN)_5NO]$ units to show thermally-induced rotational vibrations (Fig. 2). Then, the rotational vibration causes the NTE as observed. In the 3D system, however, the steric hindrance suppress the rotational vibration. Then, the inherent PTE overcomes the NTE behavior.

In the out-of-plane components (Fig. 6b), the magnitude of PTE increases with decrease in the dimensionality. This is because the chemical bonds between the cyano-bridged layers become weaker as the dimensionality decreases. Actually, the number N of the cyano-bridge per one $[Fe(CN)_5NO]$ between the layers decrease from 1.67 ($= 2 \times (5/6)$) for the 3D system, 1 for the distorted-3D system, and 0 for the 2D system. The reduction of the cyano-bridge weakens the inter-layer interaction, and enhances the PTE behavior.
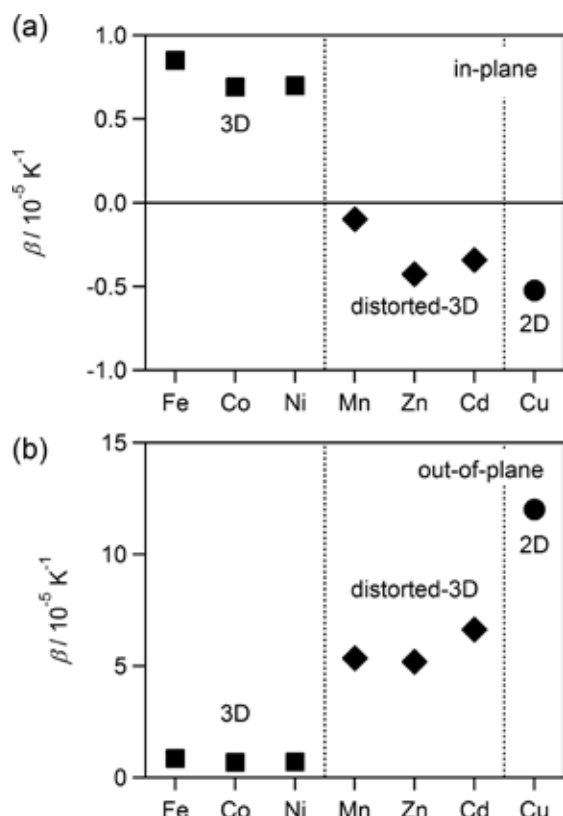

Fig. 6 (a) In-plane, and (b) out-of-plane components of the thermal expansion against M_A for $M_A[Fe(CN)_5NO]\cdot zH_2O$. The **Fe**, **Co**, and **Ni** compounds with 3D network (closed squares), the **Mn**, **Zn**, and **Cd** compounds with distorted- 3D network (closed diamonds), and the **Cu** compound with 2D network (closed circles).

Conclusions

In conclusion, we demonstrated that the anisotropic thermal expansion properties of the metal nitroprussides significantly depend on the dimensionality of the network structure. The dimensionality dependence of the thermal expansion is well explained by the rotational vibrations of $[Fe(CN)_5NO]$ units as well as their steric hindrances. Here, we emphasize that the metal nitroprussides is a unique system, in which the dimensionality of the cyano-bridged transition metal network can be controlled by chemical substitution of the M_A site.

Acknowledgements

Notes and references

[a] Graduated School of Pure and Applied Science, University of Tsukuba, Tsukuba, Ibaraki 305-8571, Japan. Fax: +81 29 853 4337; Tel: + 81 29 853 4337; E-mail:moritomo@sakura.cc.tsukuba.ac.jp

[b] JASRI/SPring-8, 1-1-1 Kouto, Sayo-cho, Sayo-gun, Hyogo 679-5198, Japan.

† Electronic Supplementary Information (ESI) available: Temperature dependences of magnified X-ray powder diffraction patterns. See DOI: 10.1039/b000000x/

1   T. A. Mary, J. S. O. Evans, T. Vogt and A. W. Sleight, *Science*, 1996, **272**, 90.

2   A. L. Goodwin, M. Calleja, M. J. Conterio, M. T. Dove, J. S. O. Evans, D. A. Keen, L. Peters and M. G. Tucker, *Science*, 2008, **319**, 794.

3. Y. Wu, A. Kobayashi, G. J. Halder, V. K. Peterson, K. W. Chapman, N. Lock, P. D. Southon and C. J. Kepert, *Angew. Chem., Int. Ed.*, 2008, **47**, 8929.

4   S. Margadonna, K. Prassides and A. N. Fitch, *J. Am. Chem, Soc.*, 2004, **126**, 15390.

5   K. W. Chapman, P. J. Chupas and C. J. Kepert, *J. Am. Chem, Soc.*, 2006, **128**,7009.

6   T. Matsuda, J.E. Kim, K. Ohoyama and Y. Moritomo, *Phys. Rev. B*, 2009, **79**, 172302.

7   J. S. O. Evans, Z. Hu, J. D. Jorgensen, D. N. Argyriou, S. Short and A. W. Sleight, *Science*, 1997, **275**, 61.

8   C. A. Perottoni and J. A. H. da Jornada, *Science*, 1998, **280**, 886.

9   R. Mittal, S. L. Chaplot, H. Schober and T. A. Mary, *Phys. Rev. Lett.*, 2001, **86**, 4692.

10 A. Ludi and H. U. Güdel, *Struct. Bonding*, 1973, **14**, 1.

11 E. Nishibori, M. Takata, K. Kato, M. Sakata, Y. Kubota, S. Aoyagi, Y. Kuroiwa, M. Yamakata and N. Ikeda, *Nucl. Instrum. Methods Phys. Res. A*, 2001, **467-468**, 1045.

12 F. Izumi and K. Momma, *Solid State Phenom.*, 2007, **130**, 15.

13 L. Reguera, J. Balmaseda, C. P. Krap and E. Reguera, *J. Phys. Chem. C* 2008, **112**, 10490.

14 J. B. Ayers and W. H. Waggoner, *J. Inor. Nucl. Chem.*, 1969, **31** 2045.

15 D. B. Brown, *Inorg. Chem.*, 1975, **14**, 2582.

16 L. A. Gentil, E. J. Baran and P. J. Aymonino, *Inorg. Chim. Acta*, 1976, **20**, 251.

17 J. C. Long, J. L. Thomas and J. C. Lombardi, *J. Inorg. Nucl. Chem.* 1978, **40**, 1627.

18 D. F. Mullica, E. L. Sappenfield, D. B. Tippin and D. H. Leschnitzer, *Inorg. Chim. Acta*, 1989, **164**, 99.

19 D. F. Mullica, D. B. Tippin and E. L. Sappenfield, *Inorg. Chim. Acta*, 1990, **174**, 129.

20 D. F. Mullica, D. B. Tippin and E. L. Sappenfield, *J. Coord. Chem.*, 1992, **25**, 175.

5 21 E. Reguera, J. F. Bertrán, J. Miranda and A. Dago, *Hyperfine Interact.*, 1993, **77**, 1.

22 E. Reguera, A. Dago, A. Gómez and J. F. Bertrán, *Polyhedron*, 1996, **15**, 3139.

23 Z. Z. Gu, O. Sato, T. Iyoda, K. Hashimoto and A. Fujishima, *Chem.*
10 *Mater.*, 1997, **9**, 1092.

24 A. Benavente, J. A de Morán, O. E. Piro, E. E. Castellano and P. J. Aymonino, *J. Chem. Cryst.*, 1997, **27**, 343.

25 N. Machida, S. Ohkoshi, Z. J. Zhong and K. Hashimoto, *Chem. Lett.*, 1999, 907.

15 26 A. Gómez, E. Reguera and L. M. D. Cranswick, *Polyhedron*, 2001, **20**, 165.

27 J. Balmaseda, E. Reguera, A. Gomez, J. Roque, C. Vazquez and M. Autie, *J. Phys. Chem. B*, 2003, **107**, 11360.

28 M. Zentková, M. Mihalik, I. Tóth, Z. Mitróová, A. Zentko, M.
20 Sendek, J. Kováč, M. Lukáčová, M. Maryško and M. Miglierini, *J. Mag. Mag. Mater.*, 2004, **272-276**, e753.

29 J. T. Culp, C. Matranga, M. Smith, E. W. Bittner and B. Bockrath, *J. Phys. Chem. B*, 2006, **110**, 8325.

30 E. Torres-Garcia, J. Balmaseda, L. F. del Castillo and E. Reguera, *J.*
25 *Therm. Anal. Calo.*, 2006, **86**, 371.